Available online at www.sciencedirect.com
ScienceDirect
Russian Geology and Geophysics 52 (2011) 650–667
RUSSIAN GEOLOGY AND GEOPHYSICS
www.elsevier.com/locate/rgg

Slab shape in subduction zones beneath the Kurile–Kamchatka and Aleutian arcs based on regional tomography results

I.Yu. Koulakov [a,*], N.L. Dobretsov [b], N.A. Bushenkova [a], A.V. Yakovlev [a]

[a] *A.A. Trofimuk Institute of Petroleum Geology and Geophysics, Siberian Branch of the Russian Academy of Sciences, pr. Akademika Koptyuga 3, Novosibirsk, 630090, Russia*
[b] *V.S. Sobolev Institute of Geology and Mineralogy, Siberian Branch of the Russian Academy of Sciences, pr. Akademika Koptyuga 3, Novosibirsk, 630090, Russia*

Received 15 September 2010; accepted 9 November 2010
Available online xx May 2011

Abstract

A 3-D model of the seismic heterogeneities of *P*- and *S*-velocities has been constructed down to 1100 km beneath the Kurile–Kamchatka and Aleutian subduction zones on the basis of the regional tomographic inversion of data from global seismic catalogs. Particular attention is paid to verifying the data by different tests. A clear image of a classic subducting oceanic slab is observed along the entire Kurile–Kamchatka arc, which coincides in the *P*- and *S*-models and with the distribution of deep seismicity. These data served as a basis for a parametric model of the upper and lower slab boundaries beneath the Kurile–Kamchatka arc. According to this model, the slab has various thicknesses and maximum penetration depths in different arc segments. In the southern part of the arc, between depths of 600 and 700 km, the slab moves horizontally and does not penetrate the lower mantle. Beneath the North Kuriles and southern Kamchatka, it subducts down to 900 km. These data suggest that the subducting slab becomes a viscous and nonelastic body and the changes in its shape may be due to phase transitions with increasing temperature and pressure. We attribute its gentler dipping and thickening beneath the South Kuriles to the oceanic "pushing" mechanism. The lithospheric thinning, steeper subsidence, and penetration into the lower mantle beneath the North Kuriles are due to the predominant "gravity sinking," or "slab pull," mechanism.

Unlike some other researchers, we have obtained a high-velocity anomaly beneath the western Aleutian arc (not as clear as beneath the Kurile–Kamchatka arc, yet quite reliable). It suggests the presence of a slab subducting down to 200–250 km. In the eastern Aleutian arc, we clearly observe the Pacific slab subducting down to 500–600 km (somewhat deeper than in the previous studies).

Keywords: seismic tomography; mantle; Kurile–Kamchatka arc; Aleutian arc; subduction

Introduction

Subduction zones, which demarcate active oceanic margins, are associated with the most intense geodynamic processes on the Earth. Here, the highest plate-convergence rate is observed (can exceed 10 cm/yr). Strong deformations accompanied by fluid and melt migrations in the crust and mantle within a relatively narrow zone at the plate boundary cause extremely intense mechanical and chemical processes. These processes are responsible for the diversity of geological structures in subduction complexes. The vast majority of volcanic eruptions and large earthquakes occur in subduction zones and are, apparently, related to the processes in the subducting slab. Studying the relationship between these phenomena is an important objective, which attracts many geoscientists.

The general concept of subduction is confirmed by ample evidence and accepted by most experts. According to the plate-tectonics theory, an oceanic lithospheric plate originates near midocean ridges and thickens gradually while moving toward oceanic margins. In the subduction zone, this cold oceanic plate sinks into the mantle driven by convection flows (thermal and gravity instability). In this case the subsiding lithosphere undergoes structural and compositional transformations with changing *PT*-conditions. This releases the fluids, which migrate upward from the subducting oceanic plate and cause partial melting of the rocks in the overlying mantle wedge and crust. These processes are responsible for volcanic-arc formation along active oceanic margins and seismicity at great depths. However, there are alternative explanations for deep seismicity. For example, Sharapov et al. (1984) deny the

* Corresponding author.
E-mail address: KoulakovIY@ipgg.nsc.ru (I.Yu. Koulakov)

existence of subduction and explain deep seismicity by oscillating deformations owing to subhorizontal compression between continental and oceanic segments of the tectonosphere.

Although there is relative consensus about the general subduction scenario, the details of this process are actively discussed and debated. A lot of questions remain open; answering them requires new data and additional studies. For example, it is not always possible to describe subduction by a 2-D model of a descending "conveyor." The distribution of deep seismicity and the existing seismic-tomography models demonstrate that the subduction system can show wide lateral variations. The causes of the latter are a matter of heated discussion. The extremely heterogeneous composition of lavas in arc volcanoes on active oceanic margins also invites questions. Considerably different compositions can be observed in volcanoes tens of kilometers apart or even in the same volcano at different developmental stages.

The present study focuses on the Kurile–Kamchatka and Aleutian arcs (northwestern Pacific). In terms of global plate tectonics, the recent geodynamics of the study region is controlled by the convergence of the Eurasian, Okhotsk, North American, and Pacific Plates (Fig. 1). The plate boundaries in Fig. 1 are a result of many studies, which has recently been refined by large-scale GPS measurements (Kogan et al., 2000; Steblov, 2004) as well as topographic, bathymetric, and seismic analysis. The existence of the Okhotsk microplate, which is isolated from the North American Plate, is confirmed by the slip vectors (Seno et al., 1996) obtained from the focal mechanisms of earthquakes. The Okhotsk Plate can be subdivided into two parts (Bogdanov and Dobretsov, 2002). The first one, the Kamchatka–Okhotsk block (KOB) in the north, is composed of continental rocks. Along with the Sea of Okhotsk basin, it includes a continental-lithosphere area of the Kamchatka Peninsula. Subduction under Kamchatka is quite similar to the Andean subduction, where the oceanic lithosphere also subducts under the continent. The second one is the Okhotsk block (OB) in the southern Sea of Okhotsk. It is a backarc basin with well-pronounced spreading areas. Originally, this block consisted of products of oceanic-structure accretion, which took place as the subduction zone migrated.

In the Commander–Aleutian (northern) part of the study region, we distinguish the Bering block (BB) and the Western basin (WB), which are separated by the Olyutor Ridge. The BB is an accretionary block structurally similar to the OB. The WB borders in the south on the Commander Islands shear zone, where no manifestations of arc volcanism were found. The BB has a small segment separated by the Bauer Ridge which appears to be the more ancient extension of the Aleutian arc.

The deep interior structure beneath the study region was discussed in numerous works based on different approaches and data types. Geological and geophysical studies were conducted in the Kurile–Kamchatka region as early as 1957–1959. In this period the crust beneath the offshore areas around Kamchatka was studied by deep seismic sounding along with aeromagnetic and marine gravity surveying. These studies enabled a general understanding of the main structural patterns in the crust and distinguishing its major types (Gal'perin and Kosminskaya, 1964). In the late 1961, detailed seismological observations were started on the Kamchatka Peninsula and the Commander Islands, and they are still in progress (Fedotov et al., 1964, 1974; Gordeev et al., 1998). The active geological and geophysical studies in the Sea of Okhotsk conducted in the 1960s–1970s permitted compiling the first accurate tectonic maps of the seafloor (Bogdanov and Khain, 2000; Gnibidenko, 1979; Markov et al., 1967; Pushcharovskii et al., 1977).

One of the most efficient approaches to studying the mantle structure is seismic tomography involving natural sources (earthquakes). The general shapes of subducting slabs in the study area have been determined reliably by the existing global models (Bijwaard et al., 1998; Li et al., 2008; Zhao, 2004). However, these works show some differences which may prove crucial in explaining lateral variations in the properties of subduction zones. For example, according to the model in (Li et al., 2008), there is no clear image of the subducted slab beneath the Kuriles and Kamchatka. This is probably because too conservative strong damping parameters were used and this led to an oversmoothed solution. In our view, the most reliable model is that in (Bijwaard et al., 1998), which will be used for comparison with our results.

A regional tomographic model beneath Kamchatka down to ~200 km was constructed in (Gorbatov et al., 1997, 1999). This study was based on the analysis of traveltimes from local earthquakes. These authors found a fairly clear boundary between a high-velocity subducting slab and the overlying low-velocity mantle. However, the patchy structure of the anomalies in this model may be due to unstable inversion and high noise level in the data. Another regional study of the Kurile–Kamchatka and Aleutian regions was conducted by Gorbatov et al. (2001). It was based on the analysis of global catalogs with the help of a scheme similar to that used in the present study. On the basis of this model, they hypothesized the existence of a mantle plume at the junction of the Kamchatka and Aleutian arcs. On the basis of a similar dataset, Gorbatov et al. (2000) proposed a model for subduction-zone migration with episodic slab breakoff. Catastrophic slab breakoff beneath Kamchatka is also suggested by Levin et al. (2002) on the basis of a regional seismic tomographic S-model, which was obtained with the help of surface-wave data. The same model was used to explain the absence of the subducting slab under the eastern Aleutian arc (Levin et al., 2005). Also, we should mention the paper (Boldyrev, 2005), where, along with seismic heterogeneity, the distribution of anisotropic parameters is studied in the seismic focal zone beneath Kamchatka.

Data from temporary regional networks were used for teleseismic tomographic inversion, which was based on the traveltimes from remote earthquakes (Lees et al., 2007; Zhao et al., 2010). These authors clearly detect the upper boundary of a high-velocity slab under Kamchatka. However, quasivertical rays, which are used in teleseismic tomography, lead to a low vertical resolution. This should be kept in mind when

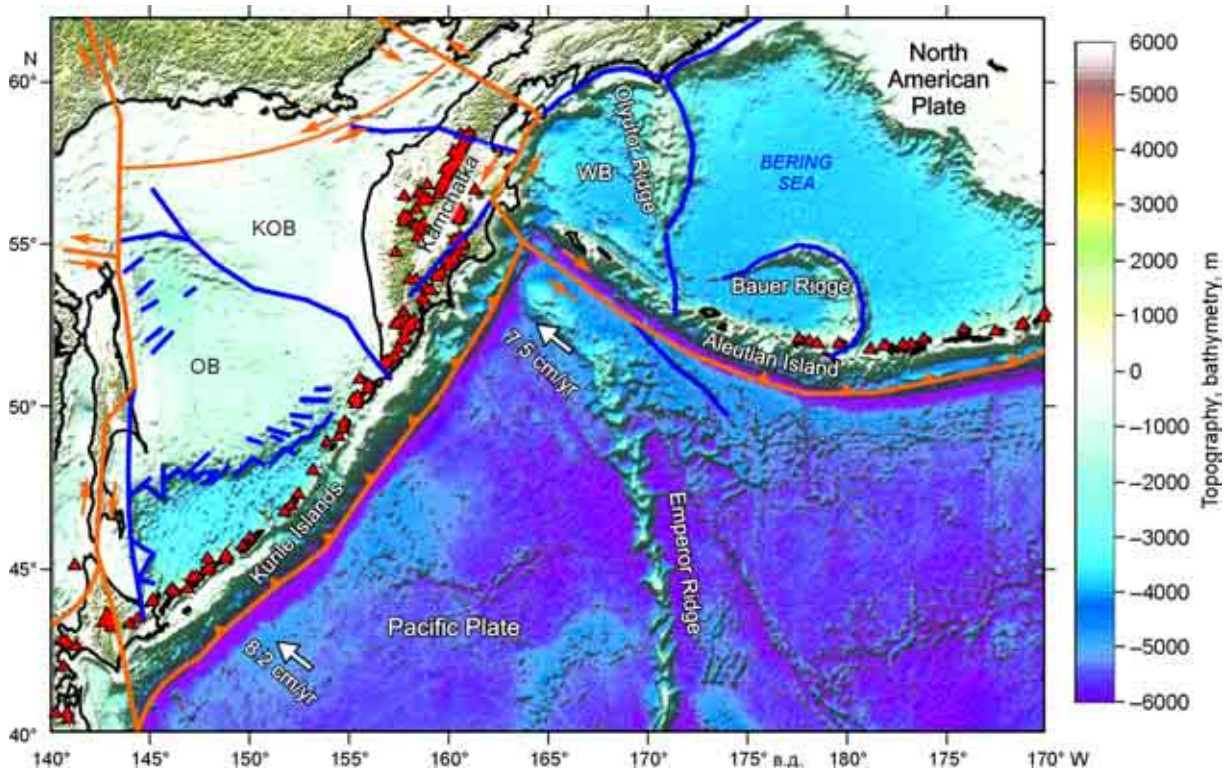

Fig. 1. Main geographical and tectonic units in the study region, with a topographic/bathymetric base map. Orange lines show tectonic-plate boundaries; violet ones were drawn by us. The movement speed of the Pacific Plate is after (Avdeiko et al., 2007; Steblov et al., 2010). Red triangles show active volcanoes after (Simkin and Siebert, 1994). WB, Western Basin; KOB, Kamchatka–Okhotsk block; OB, Okhotsk block.

interpreting the slab images in vertical sections. Data from the local networks on the Kamchatka Peninsula were also used for local crustal and uppermost mantle tomography (Nizkous et al., 2006). However, these studies are beyond the resolution of the regional scheme used in the present work.

As shown by the foregoing overview, the deep structure beneath the Kurile–Kamchatka and Aleutian arcs was studied by seismic tomography in numerous previous papers. In most of the cases, the models proposed had similar general features, but were considerably different in the details. Seismic tomography based on noisy data from natural sources is an imperfect tool. Even the processing of one data set by different authors often leads to different results. However, if several models based on different data and approaches lead to similar results, this is indirect supporting evidence for the reliability of the results.

We present models for *P*- and *S*-velocity anomalies in the mantle down to 1100 km beneath a region with the boundaries at 40°–63° latitude and 140°–190° longitude, which comprises the Kurile–Kamchatka and Aleutian subduction zones. The reliability of the structures obtained is demonstrated with the help of several different tests. Also, we compare our results with some previous models and provide a geodynamic explanation for the structures derived. These results are used for constructing the upper and lower slab boundaries beneath the Kurile–Kamchatka and Aleutian arcs as parametric 2-D surfaces.

Original data and processing algorithm

The present study uses global traveltime data on the P- and S-body waves from the catalog of the International Seismological Center (ISC, 2001) for 1964–2004. As compared with data from regional and local networks, the advantage of this catalog is the long record period and global coverage. However, the quality of the ISC data is not high enough for seismic tomography because of the abundance of defective records and the use of outdated schemes for event localization. Therefore, these data need preprocessing. The ISC data were previously redetermined in (Engdahl et al., 1998) by more sophisticated localization algorithms. We also revised the global catalog using similar approaches, but with other, less conservative, criteria for data selection. The algorithm for event localization and outlier rejection which we used for revising the ISC catalog is described in detail in (Koulakov and Sobolev, 2006). The events were localized on the basis of the spherical 1-D model AK135 (Kennett et al., 1995). The traveltimes were corrected for the station elevation, the Earth's ellipticity, and the crustal thickness according to the global model CRUST2.0 (Bassin et al., 2000).

The tomographic inversion in the present paper is performed separately in three overlapping circular areas with a radius of 10°, which cover the study area (Fig. 2). The study area was defined down to 1100 km. As demonstrated by Koulakov and Sobolev (2006), the depth/width ratio ensuring

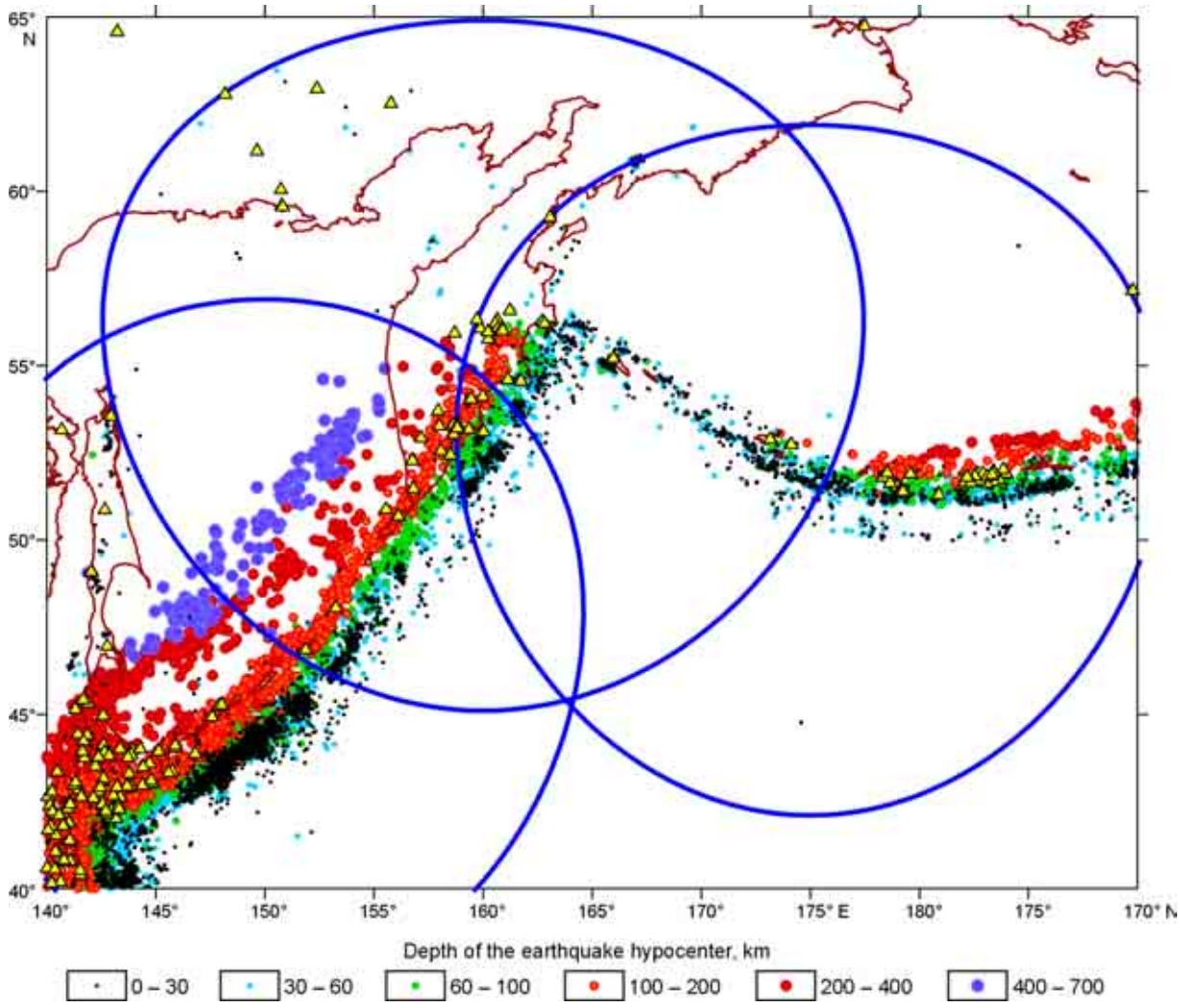

Fig. 2. Distribution of data used in the paper. Colored dots are earthquake hypocenters within the corresponding depth intervals; yellow triangles are stations from the ISC catalog; dark blue lines show the three circles where inversion was performed. Brown lines show the tectonic boundaries from Fig. 1.

the best ray intersection is 1 : 2; this determined the dimensions of the areas in our work.

Two groups of data were used for the tomographic inversion. The first one comprised the times of wave arrival from the events within the current circle, which were recorded at stations of the global network at all the possible distances. In the present paper, we used events with more than 50 recorded times. The second group comprised data from the stations in the current area which recorded remote earthquakes. In this paper, the minimum number of such stations per event was 25. In total we used ~670,000, 250,000, and 270,000 rays for each of the three areas.

Regional tomographic inversion was performed by the algorithm developed by Koulakov et al. (2002). In later works this algorithm was modified substantially and used for studying the upper-mantle structure beneath some regions: the Pamirs and Hindu Kush (Koulakov and Sobolev, 2006), Iran (Alinaghi et al., 2007), the East African Rift (Koulakov, 2007), Europe (Koulakov et al., 2009), Asia (Koulakov, 2011), and others. It is based on a linearized approach. All the calculations are done on the basis of the rays constructed in the 1-D model AK135 (Kennett et al., 1995). Note that a nonlinear algorithm with 3-D ray tracing (for example, LOTOS (Koulakov, 2009)) is quite easily adaptable for this purpose. However, this would make the calculation considerably longer, thus making it difficult to evaluate the optimum inversion parameters. The velocity distribution was set by node parametrization (Koulakov et al., 2002). In our study the nodes were installed at 15 depths (50, 100, 150, 220, 290, 360, 430, 500, 570, 640, 710, 800, 900, 1000, 1100 km). At each level the nodes were placed on parallel lines depending on the ray density. The minimum distance between the nodes is fixed in areas with high ray density. Where the ray density is below 10% of the average, nodes are not installed. To minimize artifacts related to the grid orientation, four models based on grids with different basic orientations at 0°, 22º, 45°, and 67° are calculated independently and then averaged in one model.

The first-derivative matrix A_{ij}, which is responsible for variations in the seismic velocities in the study area, is calculated along the rays constructed in the 1-D model. Along

with the distribution of *P*- and *S*-velocities, the matrix includes elements responsible for correcting the coordinates and the origin times of the sources (four parameters per source) as well as for station corrections. The matrix was inverted by the LSQR method (Paige and Saunders, 1982; van der Sluis and van der Vorst, 1987). Regularization, which ensures the smoothing of the velocity anomalies, is performed by introducing an additional matrix block. Each of its lines has two nonzero elements, 1 and –1, which correspond to the parameters at the adjacent nodes. The inversion algorithm is described in more detail in (Koulakov and Sobolev, 2006).

When performing the inversion, one faces the problem of weighting different-dimension parameters (distribution of velocities and source parameters, station corrections) and determining the smoothing parameters. This is an extremely difficult and hardly formalizable problem. In our studies the weighting parameters are estimated from synthetic tests, which were done with realistic noise and under the same inversion conditions as in case of real-data processing.

The main model in the present paper was obtained by averaging 12 inversion results (four models for each of the three circles). All of them were combined in one model

$$dV^{\text{sum}} = \sum_{i=1}^{M} C(d^{\text{cen}})\, D(d^{\text{node}})\, dV_i \Big/ \sum_{i=1}^{M} C(d^{\text{cen}})\, D(d^{\text{node}}),$$

where dV_i is the value of the velocity anomaly in the ith model; M, number of models; C, a function of d^{cen}, the distance from the center of the current circle (for distances smaller than $R/2$, where R is the circle radius, $C = 1$; for distances between $R/2$ and R, C decreases linearly from 1 to 0); D is a function of d^{node}, the distance from the nearest parametrization node in one of the grids. The values in the summary model are shown only in the areas where the distance from the nearest node does not exceed the predefined distance $d_{\min}$.

It is worth noting that the stations are nonuniformly distributed over the study region (Fig. 2). For example, along a more than 1000-km segment of the Central and North Kuriles, there are only two stations providing the data for our study. The stations are also very sparsely distributed between Kamchatka and the central Aleutian Islands. In principle, the regional tomographic scheme can operate without data from regional stations, only on the basis of the data on earthquakes in the study region recorded by the global-network stations. However, regional networks improve the accuracy of source location and the model quality. Therefore, the interpretation of results for the two above-mentioned arc segments requires particular caution. For such areas, it is especially important to take into account the results of resolution tests ("checkerboard") and the influence of random noise (test with even and odd data). The reliability problem is discussed in more detail in the next section.

Results and verification

The summary models for the *P*- and *S*-velocity anomalies are shown in 12 horizontal sections (Fig. 3, *A*, *B*). Also, we present 13 vertical sections for the Kurile–Kamchatka arc (Fig. 4) and nine across the Aleutian arc (Fig. 5). The areas with insufficient data coverage, where the distance from the nearest node of the parametrization grid exceeds 80 km, are shaded.

It is known that tomographic inversion always enables a solution. Therefore, the main objective of tomography is not to show the results of actual-data inversion but to provide convincing arguments that they reflect real structures in the Earth. To ensure satisfactory verification of the model, we have to do some tests and compare it with data from other sources.

The first informal verification criterion for tomographic models is the comparison of the independently obtained distributions of *P*- and *S*-velocity anomalies. In theory, *P*- and *S*-velocities do not always show correlation, but, in practice, large objects in the Earth are similar in *P*- and *S*- models. If the *P*- and *S*-velocity patterns show no correlation, particular attention should be paid to testing the data and algorithm. In our case the *P*- and *S*-velocity anomalies are of qualitatively similar shape, which may suggest that the inversion results are stable.

Another informal reliability criterion is comparison with geological structures whose existence was proven on the basis of independent sources. In our case it is a subducting oceanic slab, which is delineated by earthquake hypocenters in the Benioff zone. It is common knowledge that the subducting slab is considerably colder than the surrounding mantle and, correspondingly, must be manifested in a high-velocity seismic anomaly. It is seen from the vertical sections (Figs. 4, 5) that a dipping high-velocity anomaly lies along the zone of deep seismicity, exactly where the subducting slab is expected.

One of the most important verification criteria for tomographic data is comparison with the existing models obtained for the study region by other authors. In Fig. 6 we compared our result with a fragment of the global model from (Bijwaard et al., 1998), which is currently among the best ones by resolution and reliability. As the figure shows, the general features of both models coincide. Since they were obtained by different authors on the basis of different data and algorithms, such good correlation suggests that the models are highly reliable.

Also, our models show good correlation with other previous regional models. For example, the *S*-velocity distribution at a depth of 150 km in (Levin et al., 2005), which was based on surface-wave analysis, shows approximately the same structures as the distributions of *P*- and *S*-velocity anomalies at the corresponding depth obtained by us. The shape of the anomalies beneath the Kurile–Kamchatka arc calculated in (Gorbatov et al., 2000) from the analysis of the global catalogs looks very similar. However, our model yields a clearer image of the subducting slab under the Aleutian arc. In (Gorbatov et al., 2000), an elongated high-velocity anomaly is observed

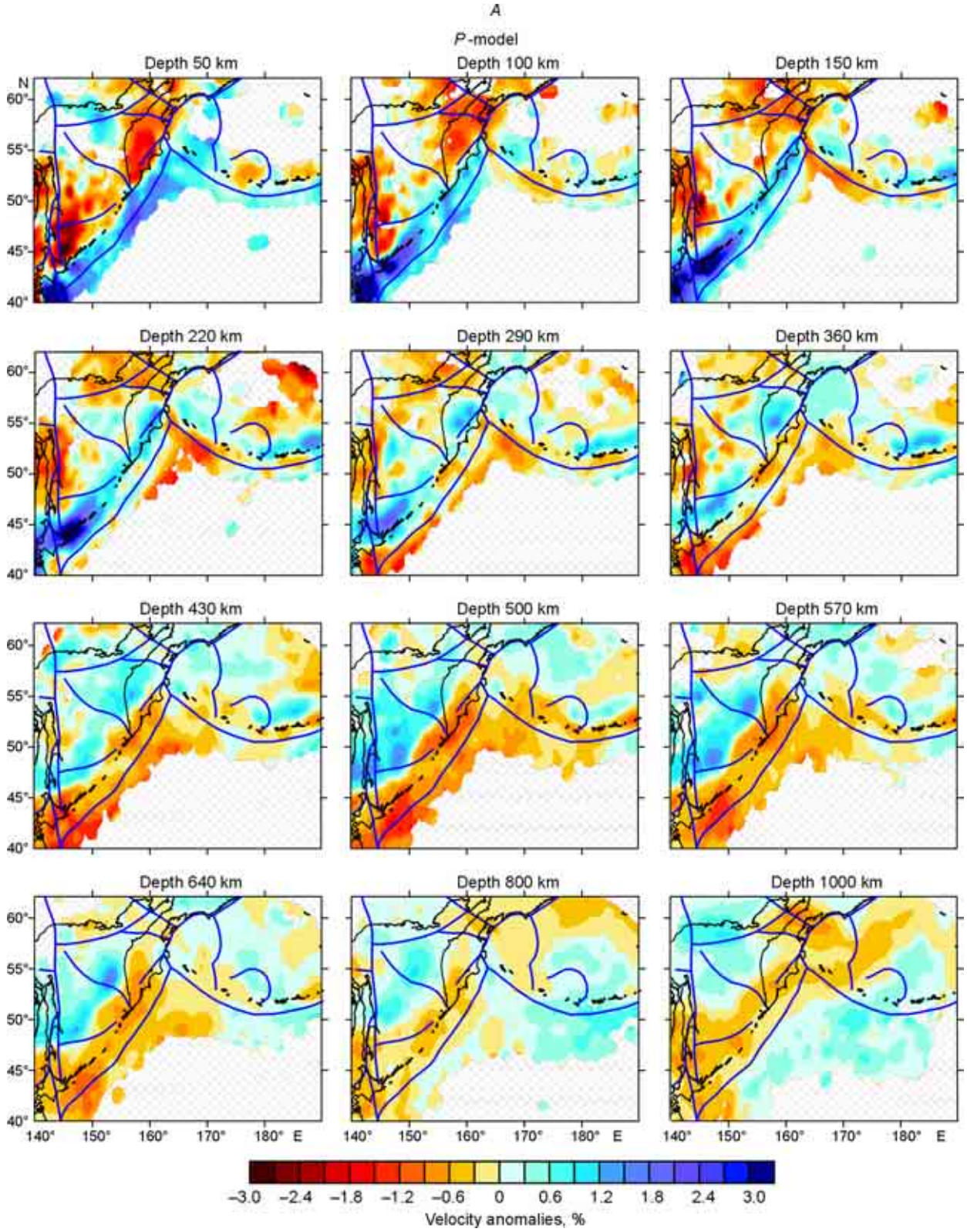

Fig. 3. Result of real-data inversion and distribution of *P*- (*A*) and *S*- (*B*) velocity anomalies at various depths. Gray areas are those with insufficient data for inversion. Violet lines show the tectonic boundaries from Fig. 1.

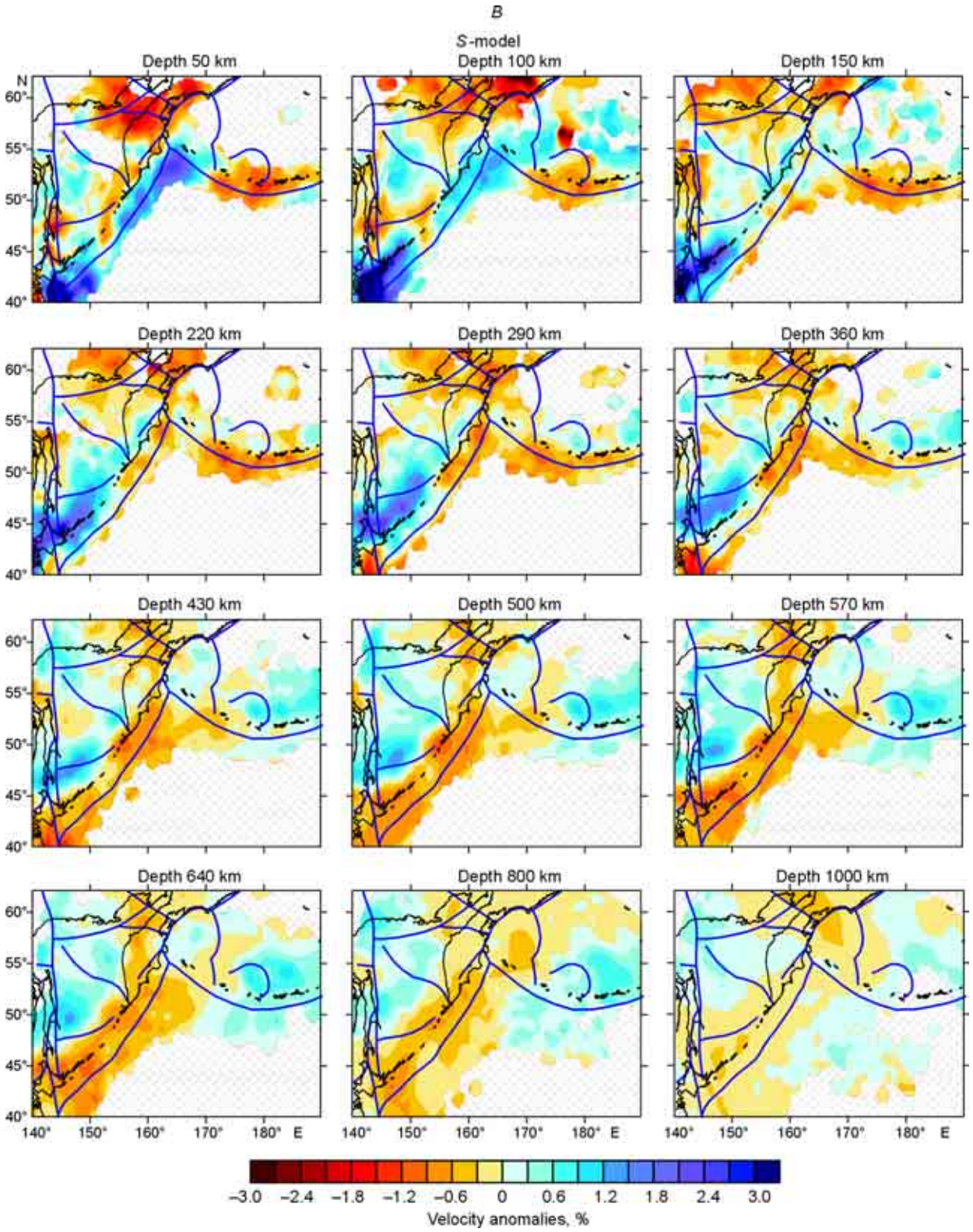

Fig. 3 (*continued*).

at depths below 700 km beneath the Kamchatka and Chukchee Peninsulas and interpreted as a remnant of a separated slab. This anomaly is also observed in our model, but it is shorter there. It is worth noting that our model included additional data from the global catalogs for ten years (1995–2004), which were not available to the authors of (Gorbatov et al., 2000).

Also, our model can be compared with the result of the regional-data inversion in (Gorbatov et al., 1999), which was obtained from the traveltimes from local earthquakes recorded

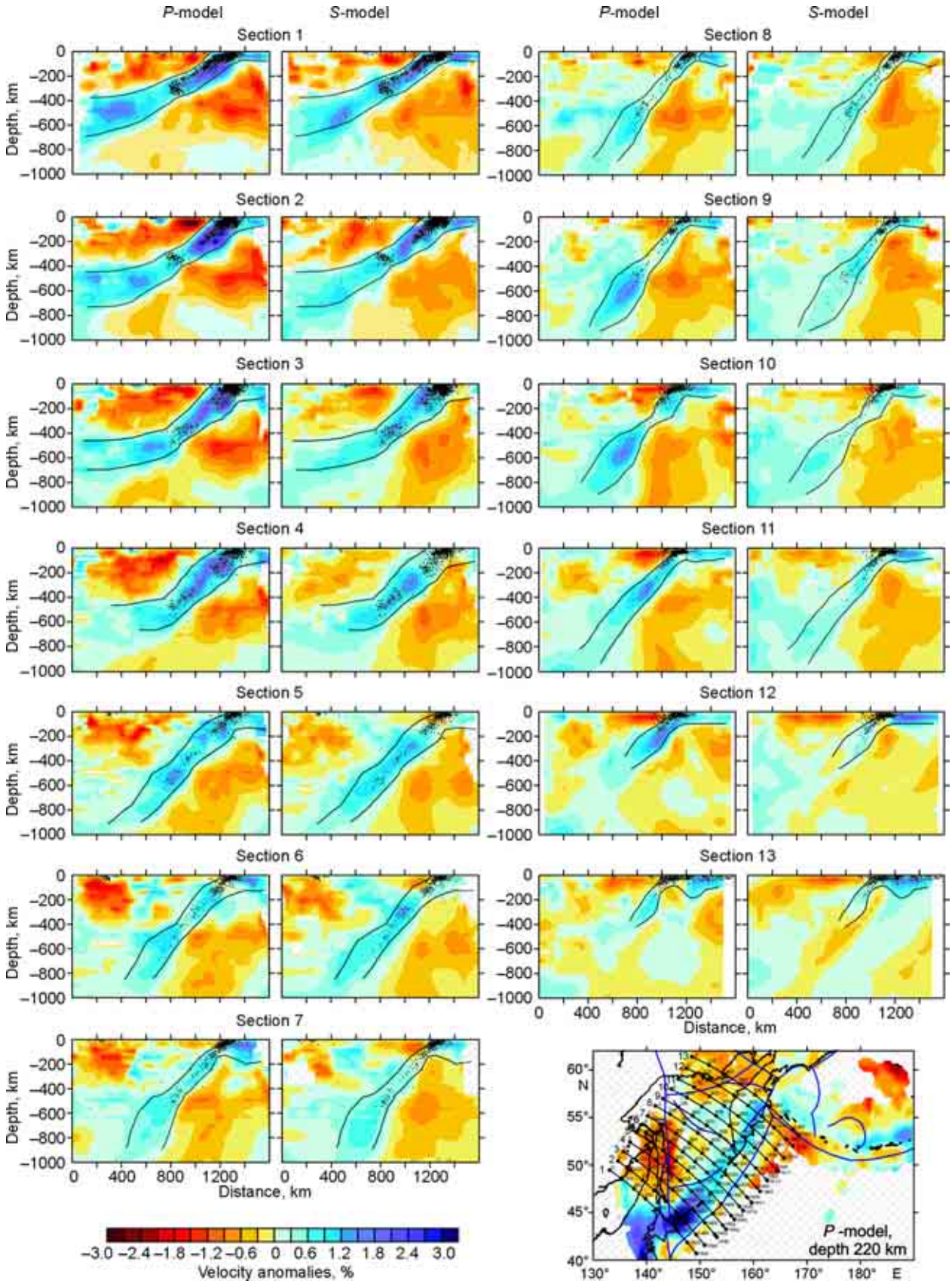

Fig. 4. Result of real-data inversion and *P*- and *S*-velocity anomalies in vertical sections across the strike of the Kurile–Kamchatka arc. Lines show the upper and lower slab boundaries. Dots are earthquake hypocenters along a strip no more than 50 km from the profile. The position of the sections is shown in the bottom right-hand corner of the map.

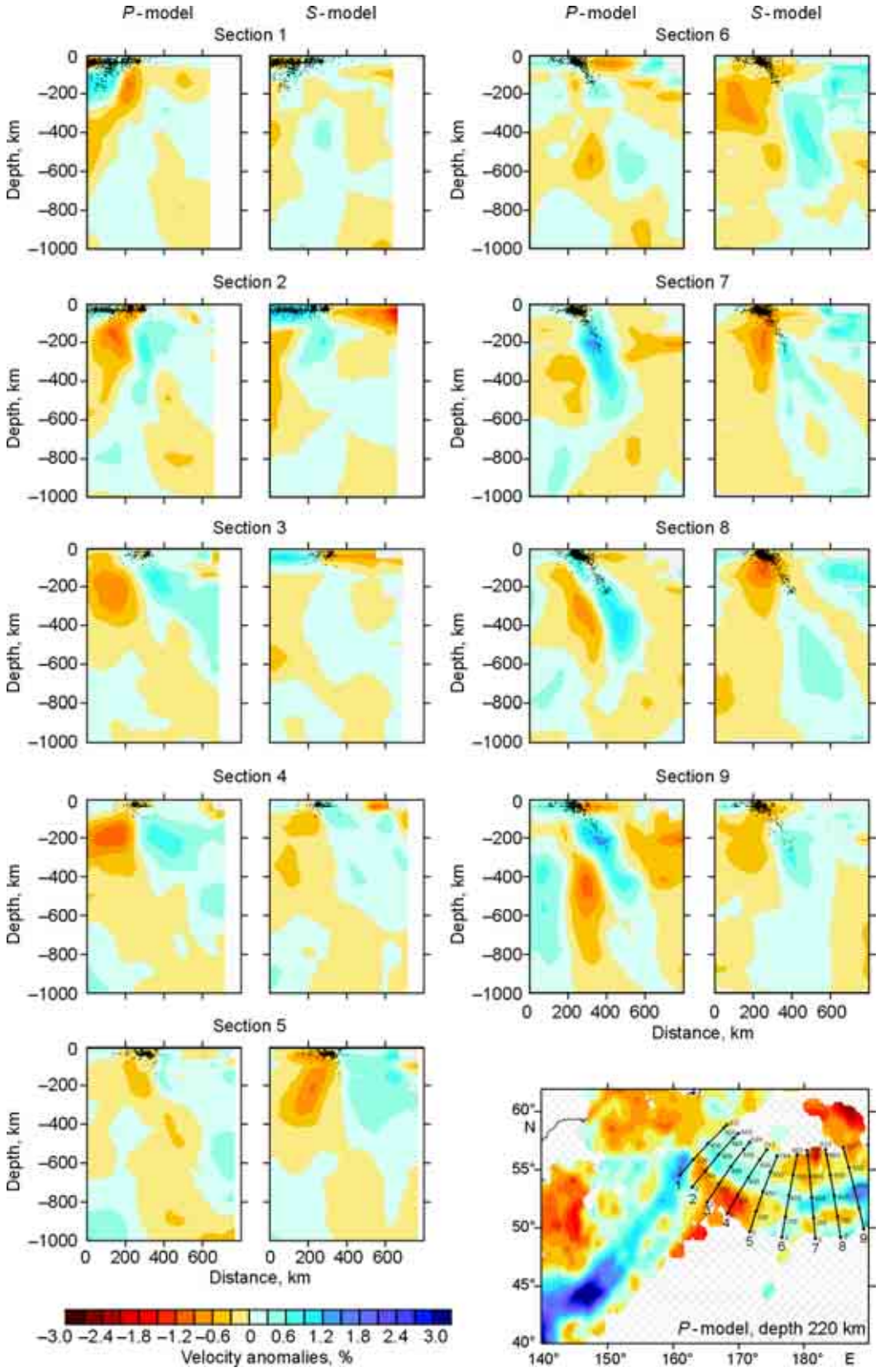

Fig. 5. Result of real-data inversion and *P*- and *S*-velocity anomalies in vertical sections across the strike of the Aleutian arc. Dots are earthquake hypocenters along a strip no more than 50 km from the profile. The position of the sections is shown in the bottom right-hand corner of the map.

by the Kamchatkan stations. This paper clearly demarcates the boundary between a high-velocity anomaly in the west and a low-velocity one under the continent, which is interpreted as the upper slab boundary. In our paper this boundary is similar: at a depth of 100 km, it passes under the eastern coast of Kamchatka; at a depth of 200 km, it shifts ~150 km deep into the peninsula. Comparison with the previous results shows that the models are highly reliable, and this permits using their quantitative characteristics for interpretation.

As pointed out above, the ISC data are very noisy. Although efforts were made to preprocess them and reject those with serious error, the noise is not eliminated and can play a substantial role in the inversion. The level of incoherent noise can be estimated from the residual decrease after the inversion. In our case the residuals of the *P*-wave traveltimes decreased by ~50%, whereas those of the *S*-wave traveltimes decreased only by 30–35%. This is higher than the values yielded by the regional models for Asia (Koulakov and Sobolev, 2006; Kulakov, 2008). The considerable decrease in the residuals in the present paper can be explained by the presence of large-scale high-contrast anomalies in the subduction zones, which generate large time anomalies and increase the signal-to-noise ratio.

The influence of random noise on the result of tomographic inversion is estimated by a test with even and odd sources (Koulakov and Sobolev, 2006). All the data in this test are divided randomly into two equal groups, for example, with even and odd source numbers. Afterward complete inversion is performed for these subsets and comparison is drawn. If noise plays a great role, it generates random anomalies, which will differ in two independent subsets. When the test results are compared, the anomalies which are not repeated in two models may prove unreliable and therefore require careful interpretation. The results of the test with even and odd events for the *P*- and *S*-models in our case are shown in Fig. 7. All the large-scale anomalies are resolved similarly in both models, and this is evidence for their reliability. The smaller-scale anomalies, which show differences, are, in all probability, accidental and have to be neglected in the interpretation. We consider only the anomalies distinguished reliably in both models.

The spatial resolution of the model is estimated by the synthetic "checkerboard" test. We use a synthetic model with alternating rectangular positive and negative anomalies. In the *P*-model, the lateral cell size was $2^\circ \times 2^\circ$; in the *S*-model, $3^\circ \times 3^\circ$. The sign of the anomalies was reversed with depth (every 200 km): 200, 400, 600, and so on. The synthetic modeling is based on the same ray configuration as the real-data inversion. It is worth noting that we are using a linearized approach, that is, the ray paths from the 1-D model. Such approximation is aimed at shortening the calculation time and doing as many tests as possible, which is important for setting the optimum free parameters for the inversion. Random noise is superimposed on the synthetic times. Its amplitude is selected so that the residuals after the inversion decrease similarly for real and synthetic data. In our case the mean noise level was 0.4 s for the *P*-wave traveltimes and 0.8 s for those of *S*-waves. The synthetic traveltimes were processed under the same scheme and with the same free parameters as in the case of real-data inversion.

In the case of inversion in selected circular areas, part of the paths of some rays is beyond the study area, whereas the synthetic times were calculated in a model with laterally unlimited velocity anomalies. Thus, the anomalies lying beyond the study area make a contribution to the synthetic data which can be considered nonrandom noise. This test shows the influence of external anomalies on the inversion data and results. The test result in Fig. 8 demonstrates how the algorithm can separate internal (useful) from external anomalies, which are regarded as incoherent noise.

As is seen from Fig. 8, the "checkerboard" cells are restored more reliably in areas with higher ray density. Noteworthy is the vertical resolution, which is fairly good for seismic tomography. The sign reversals of the anomalies in three layers at depths of 0–200, 200–400, and 400–600 km are restored reliably. According to this test, anomalies 200, 300 km, and larger in size are restored reliably in the *P*- and *S*-models, respectively.

Note that this synthetic model was used in searching for the optimum set of the values of free parameters for the real-data inversion such as the weight of the velocity-distribution parameters, corrections for the sources and receivers, and the parameters of amplitude damping and smoothing. The optimum values of these parameters are determined so as to ensure the best restoration of the synthetic model. Thus, real-data processing alternated with synthetic simulation in search of the optimum parameters.

Model description and discussion

In this section we will give a detailed description of the *P*- and *S*-velocity anomalies obtained beneath the Kurile–Kamchatka and Aleutian regions by regional tomography (Figs. 3–5).

Anomalies beneath the Kurile–Kamchatka arc

Along the Kurile–Kamchatka arc, in the upper horizontal section, which corresponds to a depth of 50 km (Fig. 3, *A*), the lithosphere is clearly divided into the oceanic part with higher seismic velocities and the backarc lithosphere with lower seismic velocities. The boundary between these zones passes precisely through the Kuriles and near the eastern coast of Kamchatka. Such zoning can be explained by the different structure and lithospheric composition in these parts. For example, the lithosphere in the southwestern Sea of Okhotsk, apparently, consists of accretion products (Bogdanov and Dobretsov, 2002; Hindle et al., 2006) and differs considerably from the highly consolidated, cold, and relatively ancient lithosphere of the Pacific oceanic plate. An intense low-velocity anomaly is observed in the southwestern Sea of Okhotsk between Sakhalin Island and the Kurile arc. We think that it is due to abnormal lithospheric heating, which was caused by

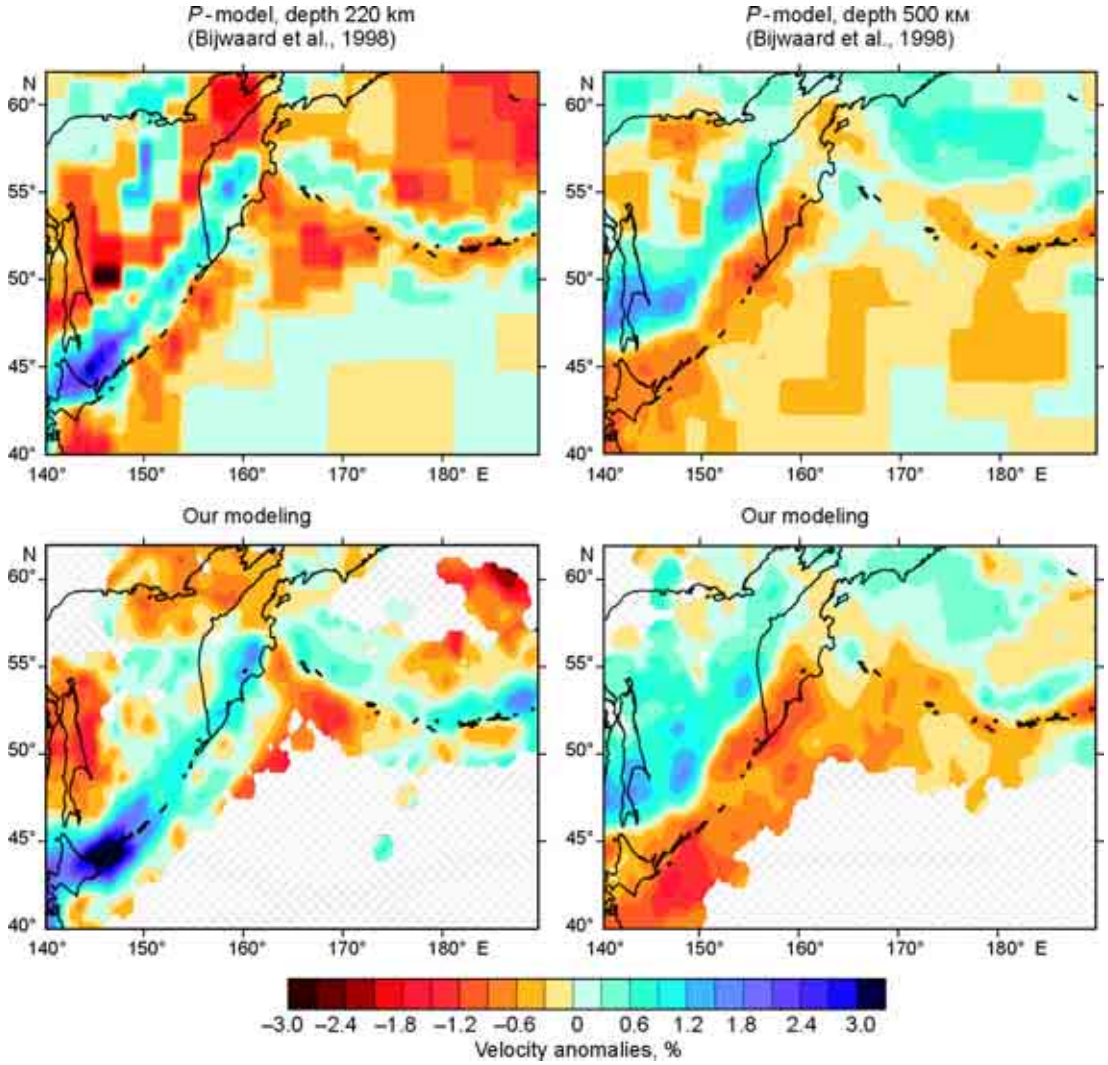

Fig. 6. Comparison of our results (upper row) with a fragment of the global model from (Bijwaard et al., 1998) (lower row). Horizontal sections are shown at depths of 220 and 500 km.

a rollback flow in the mantle wedge over the subducting slab. This flow causes spreading and gives rise to a new ocean basin with thinned lithosphere (Baranov et al., 2002). The low-velocity seismic anomaly under Kamchatka in the upper section can, apparently, be explained by the thickened crust and continental lithosphere.

At a depth of 100 km, the structure of the *P*-velocity anomalies beneath the Kurile–Kamchatka arc does not change radically (Fig. 3). Nevertheless, the high-velocity anomaly corresponding to the Pacific Plate shifts to the backarc area and becomes less uniform. Local decreases in the velocity are observed beneath the central Kurile arc. This may reflect variations in the thickness of the Pacific lithosphere; in the case of an ancient oceanic plate, these variations may be due to the influence of plumes and local roller convection cells, which heat or cool the lithosphere as it develops (Ballmer et al., 2007; Dobretsov et al., 2001).

At a depth of 150 km, the high-velocity anomaly along the Kurile–Kamchatka arc assumes the shape of a strip, except some areas where zones of elevated velocities are observed beneath the ocean (North Kuriles). These anomalies can be explained by a local thickening of the oceanic lithosphere. At a depth of 220 km, the continuous high-velocity linear anomaly corresponding to the Pacific slab under the Kurile–Kamchatka arc is the most prominent feature and shifts even farther into the backarc area.

In deeper sections (290, 360, 430 km), this anomaly is divided into two parts. The middle, where the high-velocity anomaly is the weakest, lies under the southern extremity of Kamchatka and the northern Kurile arc. Apparently, this gap is due to the fact that the slab in this part of the arc is thinner than 100 km, which is comparable with the resolution of tomographic inversion. Note that the gap lies where a local positive anomaly is observed at depths of 100–150 km near the junction between the OB and KOB. This may imply that subduction under the North Kuriles was blocked for some reason. This may have led to the accumulation of lithospheric matter in the upper part and its deficiency in the subducting slab. Another possible cause of the lithospheric thinning is the

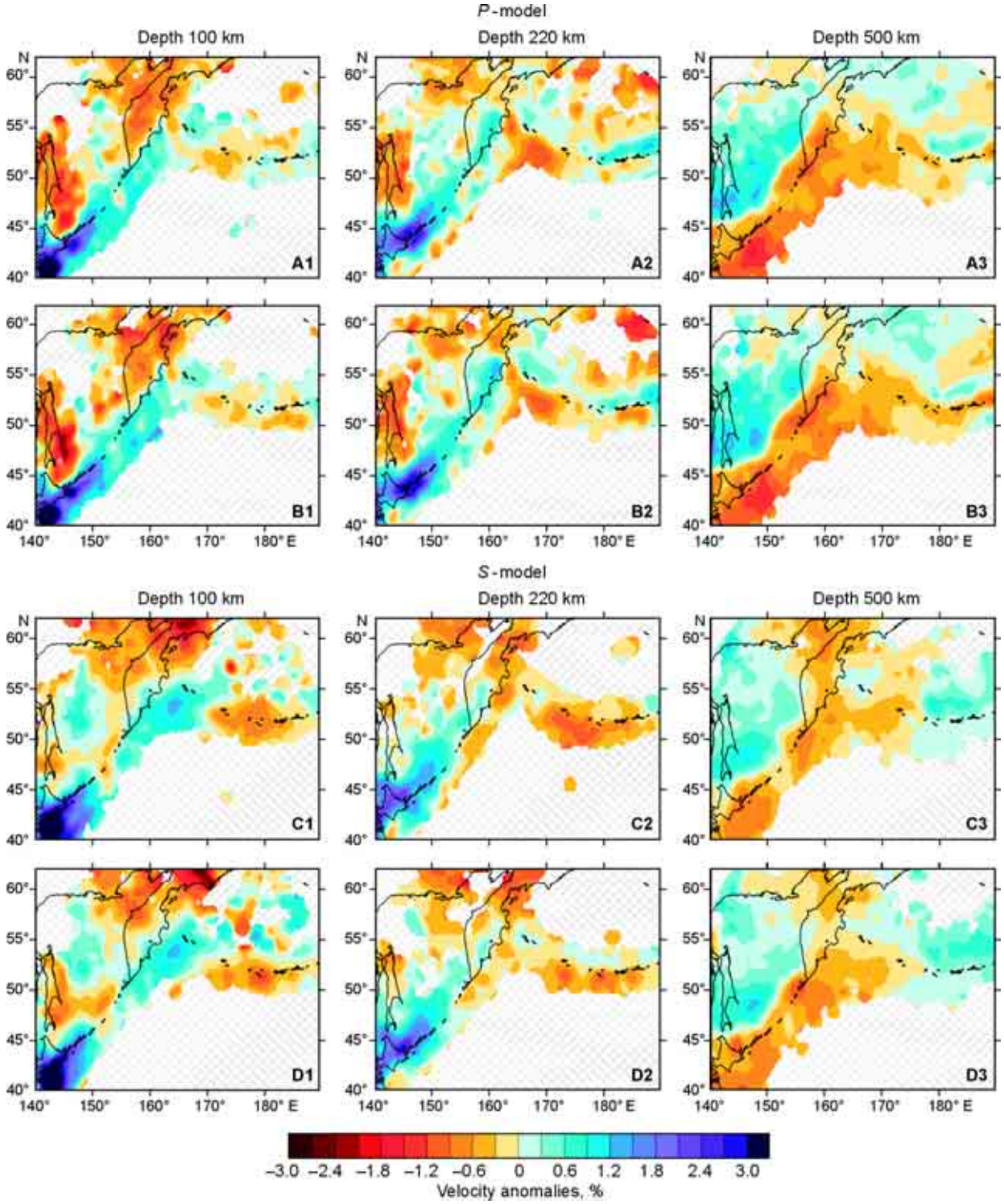

Fig. 7. Results of the test with even/odd event numbers. Columns 1, 2, and 3 correspond to depths of 100, 220, and 500 km. Row *A*, *P*-velocity anomalies, even events; row *B*, *P*-velocity anomalies, odd events; row *C*, *S*-velocity anomalies, even events; row *D*, *S*-velocity anomalies, odd events.

variable rate of the slab subduction, which will be discussed in more detail below.

In horizontal sections below 450 km, the slab under the Kurile–Kamchatka arc becomes homogeneous again. The lower slab boundary is prominent in the models, but its upper boundary is not distinguished everywhere. Note that the shape of the lower slab boundary at depths of 500–700 km coincides in the *P*- and *S*-models and correlates with the modeling in (Bijwaard et al., 1998); this suggests that the result is highly reliable.

Two alternative approaches were used for drawing the relief maps of the upper and lower slab boundaries. In the first one,

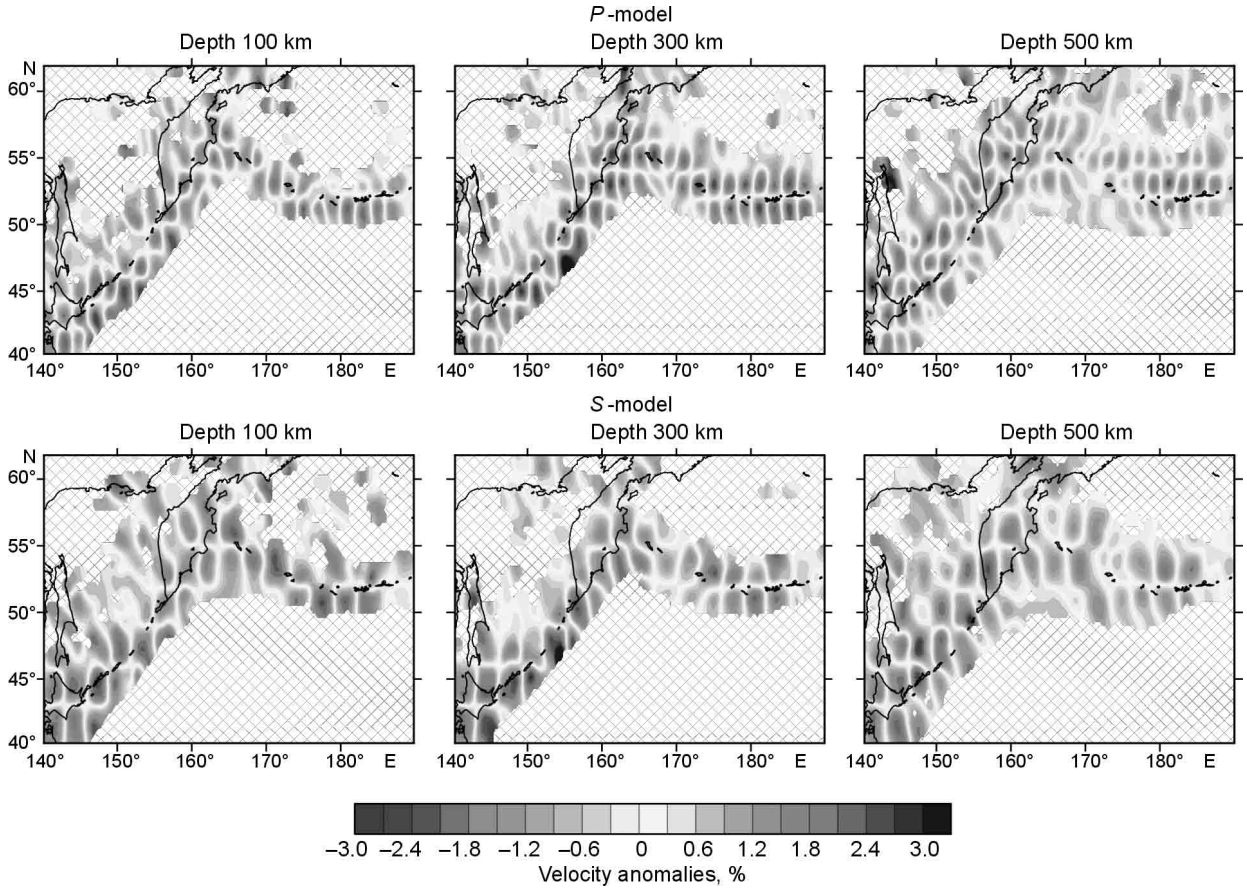

Fig. 8. Synthetic "checkerboard" test. The restoration results for *P*- and *S*-velocity anomalies are shown at depths of 100, 300, and 500 km, which correspond to the middle of the layer between the boundaries where the synthetic anomalies change their sign. The synthetic anomalies measure $2° \times 2°$ for the *P*-model and $3° \times 3°$ for the *S*-model.

the slab shape was determined by analyzing the results only in the horizontal sections of the *P*-model; in the second one, by analyzing the vertical sections of both the *P*- and *S*-models. There is a difference between these approaches concerning the result analysis. For example, in the case of linear interpolation between the vertical sections, some fine structures disappear. Also, in the second approach, the shape of the slab boundaries was simplified to ensure the best coincidence with both the *P*- and *S*-models, whereas in the first approach only the *P*-model was analyzed. Besides, the difference between the results of the slab-shape interpolation is due to the different averaging level used for visualizing the horizontal and vertical sections.

In the first approach, the relief of the upper and lower slab boundaries under the Kurile–Kamchatka arc (Fig. 9) was mapped with the help of the maps of *P*-velocity anomalies in the horizontal sections (Fig. 3, *A*). For this purpose a presumably slab-related anomaly was distinguished at each depth and its envelope was drawn along the sign-reversal line. As the figure shows, both the upper and lower slab boundaries shift to the backarc area with depth. The lower slab boundary is prominent down to 1000 km.

In the second approach, the subduction zone under the Kurile–Kamchatka arc was mapped on the basis of the vertical sections (Fig. 4). The upper and lower slab boundaries were based mainly on the analysis of *P*-velocity anomalies in the vertical sections. The distributions of seismicity and *S*-velocity anomalies were used for additional correction. One can see that the slab boundaries are superimposed quite well on the anomalies in the *P*- and *S*-models; this shows their good correlation. An algorithm was developed to convert the lines on the profile into the values on the map. These values are used for mapping the depths of the upper and lower slab boundaries in Fig. 10. These maps employ an interpolation algorithm based on linear triangulation.

The depth maps of the upper and lower slab boundaries (Figs. 9, 10) show the main features of the subduction zone along the Kurile–Kamchatka arc. The slab subducts more gently under the South Kuriles than under the central and northern Kurile arc. It subducts more gently again under central Kamchatka. Interestingly, this peculiarity correlates with the variation in its thickness at depths of 300–400 km: the thicker the slab, the more steeply it subducts. Where it subducts most steeply, the high-velocity anomaly penetrates below the 670-km discontinuity and reaches at least a depth of 900 km. No slab is observed in the lower mantle beneath the South Kuriles and central Kamchatka.

Now let us dwell upon the slab shape on the basis of the vertical sections (Fig. 4). Sections 1–3 show that, under the southern Kurile arc, the Pacific slab subducts to the transition

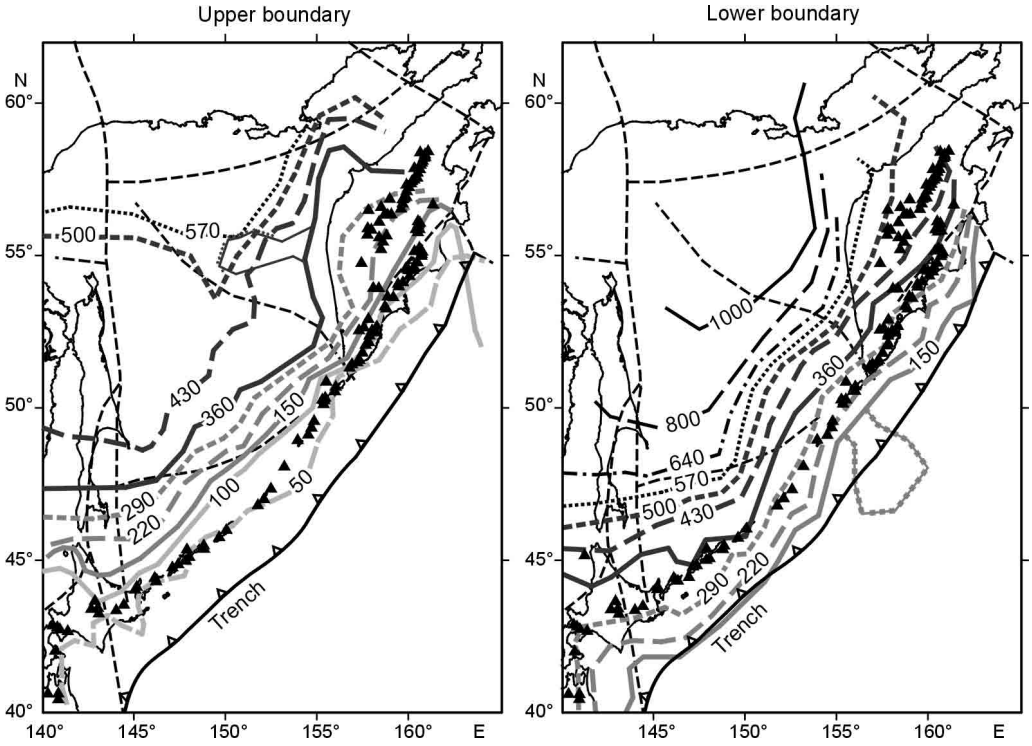

Fig. 9. Shape of the upper and lower slab boundaries, which delineate the positive *P*-velocity anomalies in the horizontal sections from Fig. 3. Numbers on the lines show the depth (km). Violet lines show the tectonic boundaries from Fig. 1. Dotted line shows presumably slab-unrelated branches of the anomaly.

zone at a constant angle and then flattens out along the upper/lower mantle boundary at a depth of 670 km. The presence of a horizontal slab in the transition zone was also demonstrated in other studies (Zhao, 2004). According to (Zhao et al., 2010), this horizontal slab part can spread for thousands of kilometers within Asia. However, since the resolution area is limited in our study, we can neither confirm nor refute this statement.

In sections 5–7, the subduction zone reshapes itself radically. The *P*- and *S*-models show clearly that the slab subducts approximately down to 900 km. It subducts more steeply and thins in its upper part, above a depth of 400 km. Also, noteworthy are some peculiarities directly unrelated to the subducting slab. For example, sections 5–6 show lowered seismic velocities under Sakhalin Island approximately down to 300 km. Under the Sea of Okhotsk, a complex pattern of high-velocity anomalies is observed, which are repeated in the *P*- and *S*-models. The origin of these structures calls for separate investigation, which we are going to conduct in the nearest future. Now we can only presume that these anomalies are due to the peculiarities of the lithosphere under the Sea of Okhotsk accretion zone. Some fragments of the previously accreted lithosphere may have thickened owing to local peculiarities (for example, in areas of underwater volcanism), and now they separate owing to gravity instability. Another cause may be the traces of the previous zones of subduction, which migrated actively in the recent geological past (Avdeiko et al., 2007; Gorbatov et al., 2000).

In sections 8–10, which run past the southern extremity of Kamchatka, the slab is not so prominent in its shallow part as in more southerly sections. This may be due to the thinner lithosphere in this arc segment. Below a depth of 400 km, the *P*-velocity anomaly in the slab is sizable and traced down to 800–900 km. In the *S*-model this peculiarity is not so well-pronounced as in the *P*-model, and this is probably due to a lack of data.

In sections 11–12, which correspond to continental Kamchatka, the upper slab part is fairly prominent. Below a depth of 600 km, a positive anomaly is observed; however, it is quite weak and of dubious reliability. Section 13 runs past the northern end of the arc, and the slab here is traced only down to 400 km. Afterward the profile leaves the subducting lithosphere.

An interesting peculiarity of the sections is the changing character of the slab-related *P*-anomalies at a depth of ~400 km. For example, the *P*-anomaly is very large and intense in sections 1–3 above this depth. It thins dramatically at a depth of 400 km, and this is accompanied by increased seismicity. This anomaly thickens again below. We think that this may be due to the reaction of the subducting slab to the phase-transition discontinuity at a depth of 410 km. In sections 6–10, the slab shape is absolutely different, but even here typical changes take place at a depth of 400 km. Above this boundary the slab seems thinner and hardly visible in the given sections, but it thickens dramatically at great depths.

The weakening of the anomaly in sections 6–10 above a depth of 400 km may be due to the lowering of the phase-transition boundary to 410 km in the area where the slab subducts. Quasivertical seismic rays, which are used in tomography, interpret this lowering as a low-velocity anomaly,

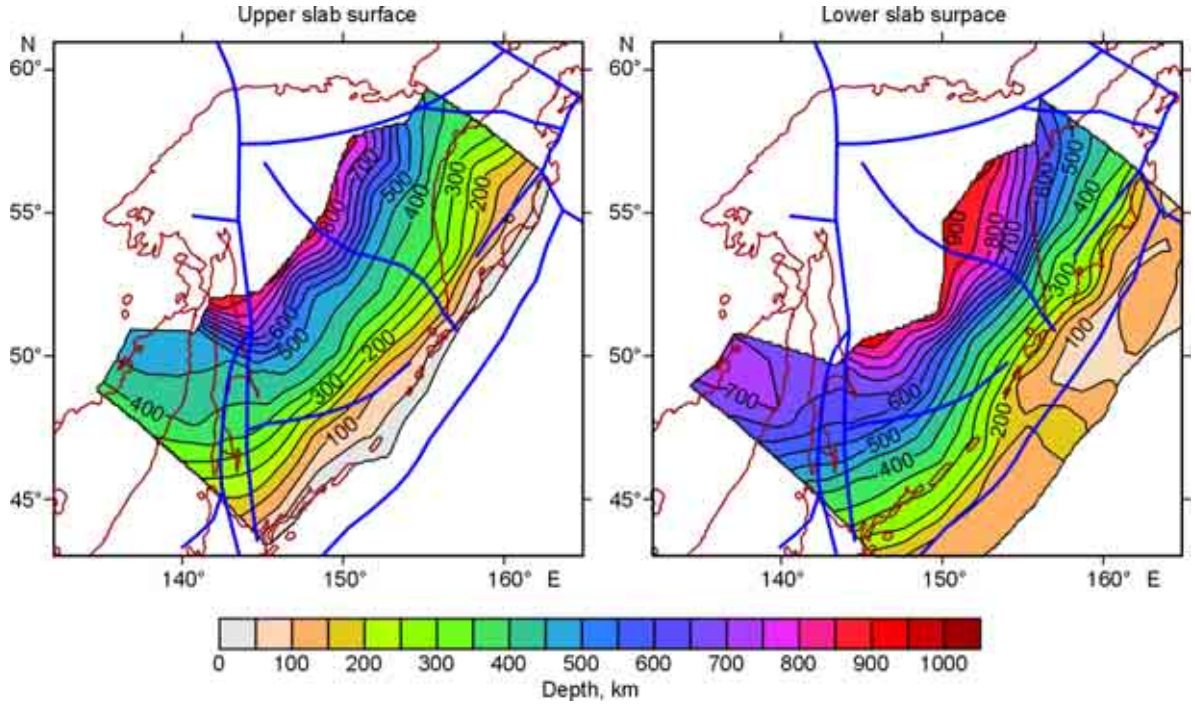

Fig. 10. Depth of the upper and lower slab boundaries under the Kurile–Kamchatka arc, determined by interpolating the slab contours from 13 vertical sections (Fig. 5). Numbers show the slab depth (km). Violet lines show the tectonic boundaries from Fig. 1.

which partly compensates for the effect of the high-velocity slab. However, our tests clearly show the variable slab thickness along the Kurile–Kamchatka arc.

Estimated rate of slab subduction under the Kurile–Kamchatka arc

The slab-thickness variations obtained in different sections can be used for estimating the subduction rates of the oceanic lithosphere. The oceanic plate before the subduction is presumed to have nearly constant thickness (no more than 70–100 km). As the subducting slab heats up, it can behave as a viscous body (boundary zones lose elasticity, and the high-velocity part of the slab thins). Also, the slab reshaping at great depths may be due to phase transitions. Besides, the oceanic lithosphere may also be stratified: it is denser and colder in the upper part and more viscous in the lower one (Fig. 11, dark and light areas, respectively). In this case the lower lithosphere may begin to deform and thicken already in the ocean, when it meets an obstacle in the form of a subduction zone. The dense part of the subducting slab heats up, and the slab probably behaves as a viscous drop rather than an elastic body starting from certain depth.

Under the principle of matter continuity, its volume passing through the section is inversely proportional to the rate. In Fig. 11 the slab-subduction rate is estimated in three most typical sections from the analysis of variations in the width of the high-velocity anomaly. For example, section 3 shows a slab which thickened dramatically (up to 200 km) just after the subduction started. The same value was obtained in most of the other models (Bijwaard et al., 1998; Zhao, 2004) and seems quite reliable, considering the large body of data. Therefore, the plate subduction has to be at least half as quick as its movement in the ocean. Thus, if a plate in the ocean moves at ~7–8 cm/yr, it subducts at a rate lower than 3–4 cm/yr. The slab thickening may be due to the fact that the subduction in this segment is caused by the "pushing" of the lithosphere from oceanward. The "slab pull" of the subsided lithosphere, which has to cause slab stretching, is not so influential in this arc segment.

The slab under the Central and North Kuriles behaves absolutely differently (Fig. 11, sections 7, 10). It has the same thickness in the upper part of the subduction zone as the oceanic lithosphere. In some places, where the slab nearly disappears from the vertical sections, it may be no thicker than 70 km, which is below the resolution of the method. It can be presumed that the "slab pull" in this arc segment, which causes the slab to thin, is key to the balance of forces. Here, the estimated rate of its subduction (8–10 cm/yr) may be higher than in the ocean. However, below a depth of 400 km, the slab thickens dramatically and subducts more slowly. Here, it probably meets an obstacle, which is marked by dramatically increased viscosity at the 670-km discontinuity (in passing from the upper to the lower mantle). This causes the subduction to slow down considerably and matter to accumulate in the transition zone between the 410- and 670-km discontinuities. When the critical mass is reached over the 670-km discontinuity, the droplike body starts to submerge into the denser and more viscous lower mantle, as is seen from the seismic tomograms of the arc center.

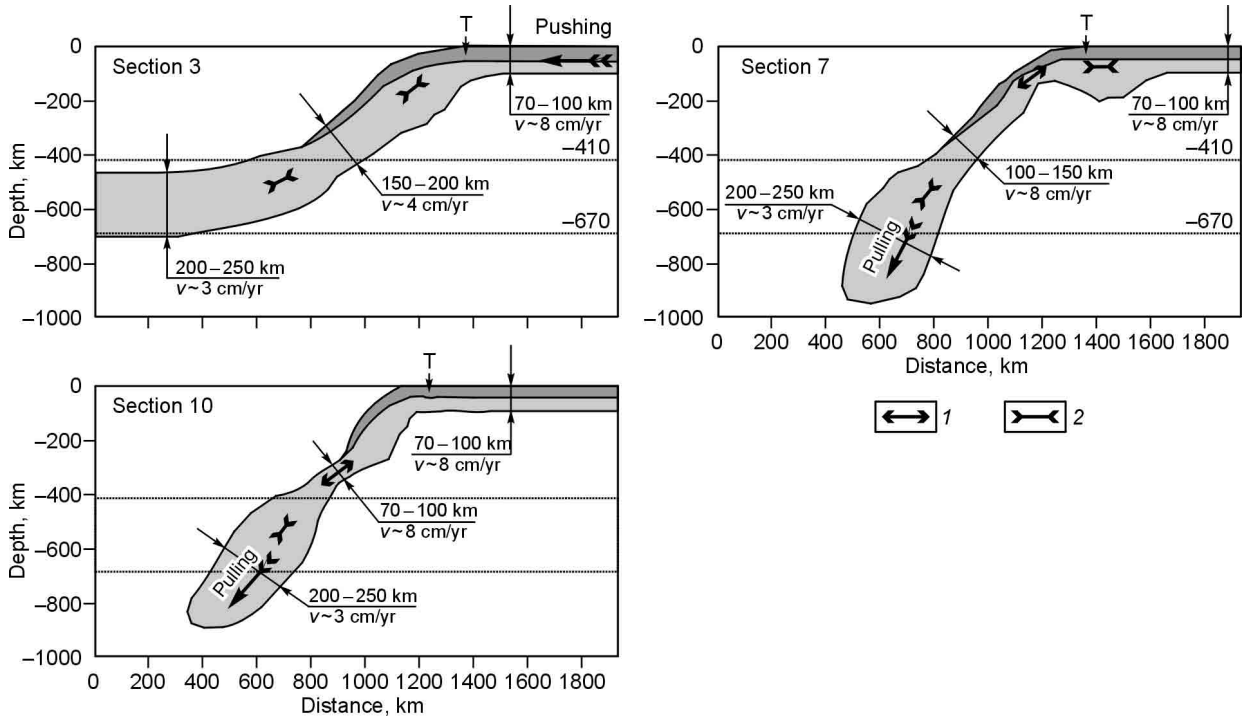

Fig. 11. Sketch map of the slab in vertical sections 3, 7, and 10 (Fig. 5). In each section the slab thickness and movement speed are roughly estimated. Arrow lettered "T" shows the position of the trench. Dark area shows the denser upper part of the slab, whose existence is discussed as a possibility in the text. *1*, extension; *2*, compression.

Anomalies beneath the Aleutian arc

The boundary along the Aleutian arc between the Pacific Plate and the backarc areas at a depth of 50 km is not so prominent in the seismic models as that along the Kurile–Kamchatka arc (Fig. 3). For example, the western Bering Sea (Western Basin) is marked by higher velocities, suggesting that it is structurally similar to the part of the Pacific Plate lying within the study region. The eastern Aleutian arc shows local low-velocity anomalies, which may reflect rollback flows in the mantle wedge over the subducting Pacific Plate.

At depths of 100 and 150 km, the *P*-velocity anomalies under the Aleutian arc change their structure radically. In the *P*-model, we see an elongated high-velocity anomaly, whose position coincides with the distribution of deep seismicity, which is caused, apparently, by the subducting slab. This anomaly is not so prominent as that along the Kurile–Kamchatka arc, but its presence is obvious at the qualitative level. Under the western Aleutian arc, we traced the slab down to 250–300 km. This positive anomaly is not prominent in the *S*-model, probably because of the considerably lower resolution, which is due to the smaller amount of data and their low quality. A local low-velocity anomaly is observed in the *P*-model at the junction of the Kamchatka and Aleutian trenches. It clearly separates the high-velocity areas corresponding to the slabs subducting under Kamchatka and the Aleutians. This anomaly is evidence that the Kamchatka and Aleutian slabs, which are parts of the Pacific Plate, are clearly separated from each other at depth.

It is worth noting that our model beneath the western Aleutians differs considerably from the seismic structures obtained by Levin et al. (2005), which are based on surface-wave analysis. These authors did not find any slab-related high-velocity anomalies there. On the contrary, Levin et al. (2005) observed a low-velocity pattern beneath the western Aleutians, which is interpreted as a slab window. This suggests massive movement of mantle matter through the "window" in the subduction zone in the western Aleutian arc. We attribute such a structural difference to the lower horizontal resolution of surface-wave tomography as compared with that in our approach. This factor "smears" the low-velocity anomaly at the junction of the Aleutian and Kamchatka arcs and "erases" the fairly weak high-velocity anomaly under the Aleutian arc. A slab is also not distinguished under the western Aleutian arc in (Gorbatov et al., 2000), probably for the same reason. The lower resolution in this study may be due to the considerably smaller amount of data as compared with that in the present study.

The existence of a slab under the western Aleutian arc is debated actively. The main problem in explaining the origin of the subduction in this area is that the movement vector of the Pacific Plate is oblique to the Aleutian trench. Thus, no normal component of this movement is observed now, and the boundary between the Pacific and North American Plates is marked only by strike-slip faults. However, the junction between the Aleutian and Kamchatka arcs is shifting northeastward, according to geological data. For example, this area lay near the southern extremity of Kamchatka at 30 Ma (Geist

and Scholl, 1994). In this case the normal component of the movement of the Pacific Plate with respect to the Aleutian trench was enough for full-fledged subduction. Apparently, the high-velocity anomaly in the western Aleutian arc shows the remnants of a now-passive subduction complex. The gradual breakoff of the cold parts of the stagnant slab in this place is discussed in (Avdeiko et al., 2007). Interestingly, the situation in Myanmar is very similar. The subduction of the Indian Plate is confirmed by the earthquake depth and seismic tomography (Huang and Zhao, 2006; Koulakov, 2011; Replumaz et al., 2010). However, the recent movements there are represented by pure strike-slip faults without movement across the junction.

In the eastern Aleutian arc, the subducting slab is traced fairly reliably in the *P*- and *S*-models, at least down to 500 km. This is deeper than estimated in (Gorbatov et al., 2000; Levin et al., 2002). In the eastern part, the normal component of the Pacific Plate movement is enough for full-fledged subduction.

Conclusions

On the basis of the ISC global seismic catalog, a model has been constructed for the seismic heterogeneity of *P*- and *S*-velocities in the mantle under the Kurile–Kamchatka and Aleutian arcs down to 1100 km. Additional data from more than decade-long observations permitted increasing the model resolution and reliability as compared with the previous studies (Bijwaard et al., 1998; Gorbatov et al., 2000). Much attention is paid to verifying the model and its comparison with the previous studies. A parametric model has been constructed for the upper and lower slab boundaries under the Kurile–Kamchatka and Aleutian arcs. It has many applications, for example, in numerical simulation.

The following peculiarities of the Kurile–Kamchatka arc have been distinguished.

1. A clear image of a classic subduction zone is observed along the entire Kurile–Kamchatka arc. It coincides in the *P*- and *S*-models and with the distribution of deep seismicity.

2. The subducting Pacific Plate has variable thickness, which peaks (over 200 km) under the South Kuriles and Japan. The slab has minimum thickness (less than 70 km) under the North Kuriles.

3. Under the continuity principle and assuming that the slab behaves as a viscous body, we estimated its subduction rate. We presume that the slab thickens if the predominant mechanism is "pushing" from oceanward and thins if the predominant mechanism is "slab pull."

4. The observed depth of the lithospheric subduction changes dramatically along the Kurile–Kamchatka arc and correlates with the character of the slab subduction estimated from its thickness. The slab does not penetrate the lower mantle when the "pushing" mechanism operates under the South Kuriles and Japan and slides horizontally along it on reaching the 670-km discontinuity. In the case of "slab pull" under the Central and South Kuriles, the denser slab matter accumulates in the transition zone and subsides slowly into the lower mantle, at least down to 900 km.

5. In the vertical sections, the slab image in the *P*-velocity anomalies is related to the position of the 410-km discontinuity. In some sections above this discontinuity, the anomalies in the slab lose their intensity. We think that, along with geodynamic causes, this result can be partly explained by variations in the depth of the 410-km discontinuity, which can serve as low-velocity anomalies compensating for the positive anomalies in the slab.

6. We distinguish the northern boundary of the slab under the Kamchatka arc, which appears to be clearly separated from the Aleutian slab.

The following conclusions can be drawn about the Aleutian arc.

1. In the western part of the arc, the Pacific Plate moves obliquely to the trench, and the normal component of the movement, which is necessary for subduction, is absent there. The previous studies (Gorbatov et al., 2000; Levin et al., 2002, 2005) denied the existence of subduction in this segment. In our model we distinguished a high-velocity anomaly, which suggests the presence of a slab subducting down to 200–250 km (not so strongly as in the Kurile–Kamchatka arc, yet quite reliably). The subduction mechanism in the case of oblique motion remains unclear. Maybe, now we observe remnant subduction, which was active when the Aleutian arc lay much farther south. A similar situation is observed in Myanmar.

2. In the eastern Aleutian arc, we clearly observe the Pacific slab subducting down to 500–600 km, which is somewhat deeper than in the previous studies. High-velocity anomalies of *P*- and *S*-velocities coincide with the distribution of deep seismicity and can be considered a reflection of a classic subduction zone.

References

Alinaghi, A., Koulakov, I., Thybo, H., 2007. Seismic tomographic imaging of *P*- and *S*-waves velocity perturbations in the upper mantle beneath Iran. Geophys. J. Int. 169 (3), 1089–1102.

Avdeiko, G.P., Savelyev, D.P., Palueva, A.A., Popruzhenko, S.V., 2007. Evolution of the Kurile–Kamchatkan volcanic arcs and dynamics of the Kamchatka–Aleutian junction, in: Eichelberger, J., Gordeev, E., Izbekov, P., Lees, J. (Eds.), Volcanism and Subduction: The Kamchatka Region. AGU Geophys. Monograph 172, Washington, DC, pp. 41–60.

Ballmer, M.D., van Hunen, J., Ito, G., Tackley, P.J., Bianco, T.A., 2007. Non-hotspot volcano chains originating from small-scale sublithospheric convection. Geophys. Res. Lett. 34 (23), ISI: 000251690300002 .

Baranov, B., Wong, H.K., Dozorova, K., Karp, B., Lüdmann, T., Karnaukh, V., 2002. Opening geometry of the Kurile Basin (Okhotsk Sea) as inferred from structural data. Island Arc 11 (3), 206–219.

Bassin, C., Laske, G., Masters, G., 2000. The current limits of resolution for surface wave tomography in North America. EOS Trans. AGU 81, F897.

Bijwaard, H., Spakman, W., Engdahl, E.R., 1998. Closing the gap between regional and global travel time tomography. J. Geophys. Res. 103 (B12), 30,055–30,078.

Bogdanov, N.A., Dobretsov, N.L., 2002. The Okhotsk oceanic volcanic plateau. Geologiya i Geofizika (Russian Geology and Geophysics) 43 (2), 101–114 (87–100).

Bogdanov, N.A., Khain, V.E. (Eds.), 2000. Tectonic Map of the Okhotsk Region, Scale 1 : 2,500,000 [in Russian]. Federal'naya Sluzhba Geodezii i Kartografii Rossii, Moscow.

Boldyrev, S.A., 2005. Seismic heterogeneity and seismic anisotropy of the lithosphere of the seismic focal zone in the Kamchatka region. Izv. Phys. Solid Earth 41 (1), 17–33.

Dobretsov, N.L., Kirdyashkin, A.G., Kirdyashkin, A.A., 2001. Deep-Level Geodynamics [in Russian]. Izd. SO RAN, Filial "GEO," Novosibirsk.

Engdahl, E.R., van der Hilst, R.D., Buland, R.P., 1998. Global teleseismic earthquake relocation with improved travel times and procedures for depth determination. Bull. Seismol. Soc. Am. 88 (3), 722–743.

Fedotov, S.A., Kuzin, I.P., Bobkov, M.F., 1964. Detailed seismological investigations in Kamchatka in 1961–1962. Izv. AN SSSR, Ser. Geofiz., No. 9, 1360–1375.

Fedotov, S.A., Tokarev, P.I., Godzikovskaya, A.A., Zobin, V.M., 1974. Detailed data on seismicity in Kamchatka and the Commander Islands (1965–1968), in: Fedotov, S.A. (Ed.), Seismicity and Earthquake Prediction, the Properties of the Upper Mantle and Their Relation to Volcanism in Kamchatka [in Russian]. Nauka, Novosibirsk, pp. 35–46.

Gal'perin, E.I., Kosminskaya, I.P. (Eds.), 1964. Crustal Structure in the Transition Zone between the Asian Continent and the Pacific Ocean [in Russian]. Nauka, Moscow.

Geist, E.L., Scholl, D.W., 1994. Large-scale deformation related to the collision of the Aleutian Arc with Kamchatka. Tectonics 13 (2), 538–560.

Gnibidenko, G.S., 1979. Tectonics of Marginal Seas in the Far East [in Russian]. Nauka, Moscow.

Gorbatov, A., Kostoglodov, V., Suárez, G., Gordeev, E., 1997. Seismicity and structure of the Kamchatka subduction zone. J. Geophys. Res. 102 (B8), 17,883–17,898.

Gorbatov, A., Domínguez, J., Suárez, G., Kostoglodov, V., Zhao, D., Gordeev, E., 1999. Tomographic imaging of the *P*-wave velocity structure beneath the Kamchatka peninsula. Geophys. J. Int. 137 (2), 269–279.

Gorbatov, A., Widiyantoro, S., Fukao, Y., Gordeev, E., 2000. Signature of remnant slabs in the North Pacific from *P*-wave tomography. Geophys. J. Int. 142 (1), 27–36.

Gorbatov, A., Fukao, Y., Widiyantoro, S., Gordeev, E., 2001. Seismic evidence for a mantle plume oceanwards of the Kamchatka-Aleutian trench junction. Geophys. J. Int. 146 (2), 282–288.

Gordeev, E.I., Chebrov, V.N., Vikulin, A.V., Levina, V.I., Sinitsyn, V.I., Yashchuk, V.V., 1998. The seismological observation system in Kamchatka (state, development, and prospects), in: The Kronotskii Earthquake of December 5, 1997, in Kamchatka: Precursors, Features, and Impact [in Russian]. KOMSP GS RAN, Petropavlovsk-Kamchatskii, pp. 12–24.

Hindle, D., Fujita, K., Mackey, K., 2006. Current deformation rates and extrusion of the northwestern Okhotsk plate, northeast Russia. Geophys. Res. Lett. 33, L02306, doi: 10.1029/2005GL024814.

Huang, J.L., Zhao, D.P., 2006. High-resolution mantle tomography of China and surrounding regions. J. Geophys. Res. 111, B09305, doi: 10.1029/2005JB004066.

International Seismological Centre, 2001. Bull. Disks 1–9 [CD-ROM]. ISC, Thatcham, United Kingdom.

Kennett, B.L.N., Engdahl, E.R., Buland, B., 1995. Constraints on seismic velocities in the Earth from travel times. Geophys. J. Int. 122 (1), 108–124.

Kogan, M.G., Steblov, G.M., King, R.W., Herring, T.A., Frolov, D.I., Egorov, S.G., Levin, V.Y., Lerner-Lam, A., Jones, A., 2000. Geodetic constraints on the relative motion and rigidity of Eurasia and North America. Geophys. Res. Lett. 27 (14), 2041–2044.

Koulakov, I.Yu., 2007. Structure of the Afar and Tanzania plumes based on the regional tomography using ISC data. Dokl. Earth Sci. 417 (8), 1287–1292.

Koulakov, I., 2009. LOTOS code for local earthquake tomographic inversion: Benchmarks for testing tomographic algorithms. Bull. Seismol. Soc. Am. 99 (1), 194–214.

Koulakov, I., 2011. High-frequency *P* and *S* velocity anomalies in the upper mantle beneath Asia from inversion of worldwide traveltime data. J. Geophys. Res. 116 (B04301), doi: 10.1029/2010JB007938.

Koulakov, I., Sobolev, S.V., 2006. A tomographic image of Indian lithosphere break-off beneath the Pamir–Hindukush region, Geophys. J. Int. 164 (2), 425–440.

Koulakov, I., Tychkov, S., Bushenkova, N., Vasilevsky, A., 2002. Structure and dynamics of the upper mantle beneath the Alpine–Himalayan orogenic belt, from teleseismic tomography. Tectonophys. 358 (1–4), 77–96.

Koulakov, I., Kaban, M.K., Tesauro, M., Cloetingh, S., 2009. *P* and *S* velocity anomalies in the upper mantle beneath Europe from tomographic inversion of ISC data. Geophys. J. Int. 179 (1), 345–366.

Kulakov, I.Yu., 2008. Upper mantle structure beneath southern Siberia and Mongolia, from regional seismic tomography. Russian Geology and Geophysics (Geologiya i Geofizika) 49 (3), 187–196 (248–261).

Lees, J.M., VanDecar, J., Gordeev, E., Ozerov, A., Brandon, M.T., Park, J., Levin, V., 2007. Three dimensional images of the Kamchatka–Pacific plate cusp, in: Eichelberger, J., Izbekov, P., Ruppert, N., Lees, J., Gordeev, E. (Eds.), Volcanism and Tectonics of the Kamchatka Peninsula and Adjacent Arcs. AGU Monograph 172, pp. 65–76.

Levin, V., Shapiro, N., Park, J., Ritzwoller, M., 2002. Seismic evidence for catastrophic slab loss beneath Kamchatka. Nature 418 (6899), 763–767.

Levin, V., Shapiro, N.M., Park, J., Ritzwoller, M.H., 2005. The slab portal beneath the Western Aleutians. Geology 33 (4), 253–256.

Li, C., van der Hilst, R.D., Engdahl, E.R., Burdick, S., 2008. A new global model for *P* wave speed variations in Earth's mantle. Geochem. Geophys. Geosyst. 9 (Q05018), doi: 10.1029/2007GC001806.

Markov, M.S., Averyanova, V.N., Kartashov, I.P., Solov'eva, I.A., Shuvaev, A.S., 1967. Meso-Cenozoic history and crustal structure of the Okhotsk region. Tr. GIN, No. 168.

Nizkous, I., Sanina, I., Kissling, E., Gontovaya, L., 2006. Velocity properties of ocean-continent transition zone lithosphere in Kamtchatka region according to seismic tomography data. Phys. Solid Earth 42 (4), 286–296.

Paige, C.C., Saunders, M.A., 1982. LSQR: An algorithm for sparse linear equations and sparse least squares. ACM Trans. on Mathematical Software 8 (1), 43–71.

Pushcharovskii, Yu.M., Melankholina, E.N., Raznitsyn, Yu.N., Shmidt, O.A., 1977. Comparative tectonics of the Bering, Okhotsk and Japan Seas. Geotektonika, No. 5, 83–94.

Replumaz, A., Negredo, A.M., Guillot, S., Villaseñor, A., 2010. Multiple episodes of continental subduction during India/Asia convergence: Insight from seismic tomography and tectonic reconstruction. Tectonophys. 483 (1–2), 125–134.

Seno, T., Sakurai, T., Stein, S., 1996. Can the Okhotsk plate be discriminated from the North American plate? J. Geophys. Res. 101 (B5), 11,301–11,315.

Sharapov, V.N., Simbireva, I.G., Bondarenko, P.M., 1984. Structure and Geodynamics of the Kurile–Kamchatka Seismic Focal Zone [in Russian]. Nauka, Novosibirsk.

Simkin, T., Siebert, L., 1994. Volcanoes of the World, 2nd ed. Geosci. Press (in association with the Smithson. Inst. Global Volcanism Program), Tucson, Ariz.

Steblov, G.M., 2004. Interaction between lithospheric plates in Northeastern Asia. Dokl. Earth Sci. 395 (2), 226–229.

Steblov, G.M., Vasilenko, N.F., Prytkov, A.S., Frolov, D.I., Grekova, T.A., 2010. Dynamics of the Kuril-Kamchatka subduction zone from GPS data. Fiz. Zemli, No. 5, 77–82.

Van der Sluis, A., van der Vorst, H.A., 1987. Numerical solution of large, sparse linear algebraic systems arising from tomographic problems, in: Nolet, G. (Ed.), Seismic Tomography (With Applications in Global Seismology and Exploration Geophysics). Reidel, Dordrecht, Chap. 3, pp. 49–83.

Zhao, D., 2004. Global tomographic images of mantle plumes and subducting slabs: insight into deep Earth dynamics. Phys. Earth Planet. Inter. 146 (1–2), 3–34.

Zhao, D., Pirajno, F., Liu, L., 2010. Mantle structure and dynamics under East Russia and adjacent regions. Russian Geology and Geophysics (Geologiya i Geofizika) 51 (9), 925–938 (1188–1203).

Editorial responsibility: M.I. Epov